Parametric polarization scattering of light in photorefractive $BaTiO_3$

S. G. Odulov and B. I. Sturman

Institute of Physics, Ukrainian Academy of Sciences
(Submitted 9 April 1992)
Zh. Eksp. Teor. Fiz. **102**, 455–471 (August 1992)

Two new types of parametric scattering of light in photorefractive $BaTiO_3$ crystals are investigated. Nonlinear scattering requires two orthogonally polarized pump beams. It is distinguished by high efficiency and nontrivial angular, polarization, and kinetic properties. Theory and experiment are in good agreement with respect to all scattering characteristics.

1. INTRODUCTION

Investigations of nonlinear optical effects in photorefractive crystals (PRCs) have recently gone through a period of advancement. There are several reasons for this. First, there is the 15–20 years of experience in studying the elementary mechanisms of photorefractive nonlinearity.[1,2] Second, interest has increased in the use of giant optical nonlinearity for diverse optical applications, such as, amplification of weak signals, adjustment of laser beams, phase conjugation, etc.[2–4] Finally, technological progress has led to the development of new materials with unique characteristics (the most important being $BaTiO_3$ crystals). The combination of these factors has manifested itself in greater diversity and higher quality of investigations. A large number of new optical schemes, realizing different optical characteristics and properties of the material, have appeared.[4,5] The description of nonlinear processes has progressed from qualitative and illustrative to quantitative in separate cases.

A distinguishing feature of PRCs is that the optical effects occurring in them are closely related to photoinduced charge-transfer processes. The changes induced in the optical permittivity $\Delta\hat{\varepsilon}(\omega)$ are proportional to the photoinduced electric field $\mathbf{E}$. Thus with each independent contribution to the photocurrent there is associated a unique contribution to the nonlinear optical susceptibility. The diversity and polarization properties of transport processes and the spatial dispersion are directly manifested in optics. The most important contributions to the nonlinear susceptibility are usually associated with drift and diffusion of photoexcited carriers or with the photogalvanic effect.[6] The inertia of charge-transfer processes gives rise to frequency degeneracy in the photorefractive nonlinearity—only light waves with very close frequencies can interact effectively.

Parametric processes in photorefractive crystals are often manifested in the form of bright rings and lines of scattered light. These processes were actually observed a long time ago (see, for example, Refs. 7 and 8), but an adequate interpretation of them has been found only in the last few years. Nonlinear scattering of the ordinary (o) [or extraordinary (e)] pump wave into two e (or o) parametric waves was first studied in Ref. 9 for $LiNbO_3$ and $LiTaO_3$ crystals. Parametric scattering of the form $oo \rightarrow eo$, in which the o pump wave engendered a pair of o- and e-waves, was identified in Ref. 10.

We have discovered and investigated two parametric processes, $oe \rightarrow oo$ and $oe \rightarrow ee$, which require two polarized propagating pump waves at different angles, and which fully realize the unique electrooptic properties of $BaTiO_3$. We have shown that the nonlinear scattering is associated with the amplification of the initial radiation, scattered by optical inhomogeneities of the sample as a result of parametric mixing of two copropagating pump waves and two conjugate components of the scattered light. The phase-matching conditions determine the specific nature of the spatial distribution of the scattering intensity.

The properties of the amplification exhibited by the scattered light (as a result of the associated parametric interactions) make it possible to construct a general theory for both processes. In the present paper the stationary state and the dynamics of the development of scattering are analyzed in detail. Attention is focused primarily on scattering under conditions when the space charge is formed by the dominant diffusion process (corresponding to an experiment with undoped $BaTiO_3$ crystals). In addition, the characteristic features of scattering are analyzed when the drift mechanism for recording in an external electric field is used. Theory and experiment are in good agreement with respect to all scattering characteristics.

2. BASIC EXPERIMENTAL OBSERVATIONS

Two coherent pump beams, one ordinary and the other extraordinary, converged at an angle $2\theta_p$, inside a $BaTiO_3$ crystal in the plane perpendicular to the optic c-axis (Fig. 1). The dimensions of the samples were $2.6\times4.4\times6.6$ mm^3 and $2\times4\times7$ mm^3. The yz entrance face was illuminated uniformly and continuously. The typical intensities were equal to several W/cm^2. There was no external electric field. The output characteristics were measured in the far scattering zone.

With short exposure times only two bright light spots, corresponding to the pump waves, were observed on the screen. As the exposure time increased, photoinduced scattering developed and saturated.[11,12] Stationary light scattering obeyed the following laws.

As long as the half-angle θ_p^{air} (in air) between the pump

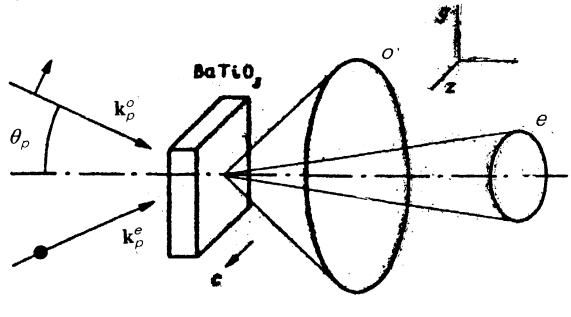

FIG. 1. Schematic diagram of the experiment.

 0038-5646/92/080241-09$05.00

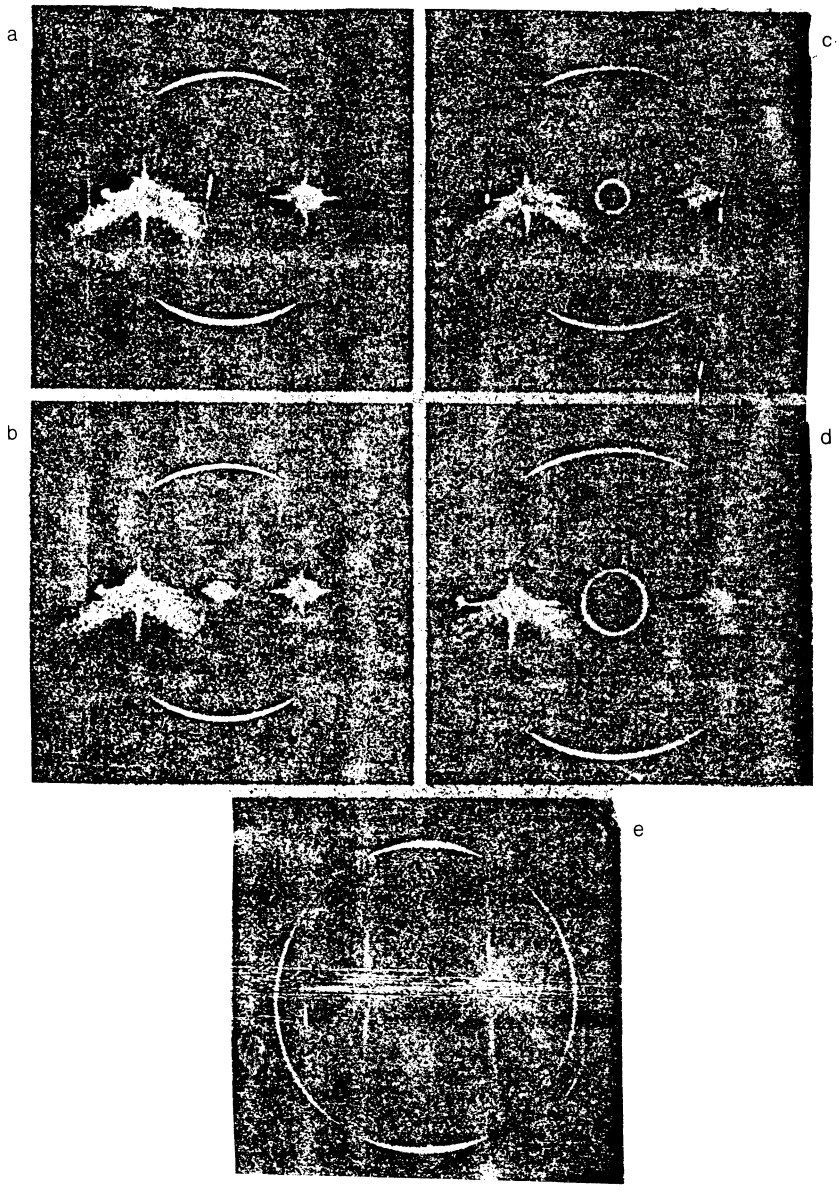

FIG. 2. Angular distributions of o and e scattering; the bright dots correspond to o and e pump beams; a, b, c, and d—stationary scattering for $\theta_p^{\text{air}} = 22$, 23, 25, and 30°; the outer ring corresponds to o waves and the inner ring in Figs. c and d corresponds to e scattering; e—typical pattern of transient o scattering for $\theta_p^{\text{air}} \approx 10°$.

beams was less than 23°, the scattered radiation corresponded to o-type waves and was concentrated primarily on the surface of a circular cone (Fig. 2).[11] The angle $2\theta_o^{\text{air}}$ of the o-wave cone increased with increasing θ_p^{air}, starting at some finite value. The intensity of the scattered waves was distributed symmetrically relative to the horizontal xy plane. The intensity was very nonuniform as a function of the azimuthal angle φ (Fig. 2a). Stationary scattering did not occur outside the plane angle formed by the vectors of the pump waves, i.e., for $|\cos\varphi| > \theta_p^{\text{air}}/\theta_o^{\text{air}}$. The maximum scattering intensity corresponded to azimuthal angles $\varphi = 90°$ and 270°. The maximum (as a function of φ) and integral scattering intensities increased rapidly with θ_p^{air}.

For angles $\theta_p^{\text{air}} > 23°$ a cone of e-polarized scattered waves was observed in addition to the cone of e-waves.[12] The angle of this cone, $2\theta_e^{\text{air}}$, increased from zero, always remaining less than $2\theta_p^{\text{air}}$ and $2\theta_o^{\text{air}}$ (Figs. 2c and 2d). The azimuthal distribution of the scattered e waves was practically uniform.

In the transient stage, conical o-scattering was also observed at azimuthal angles where there was no stationary scattering (Fig. 2e). The maximum transient scattering corresponded to $\varphi = 0$ and π. Neither stationary nor transient o scattering occurred for angles $|\cos\varphi| \approx \theta_p^{\text{air}}/\theta_o^{\text{air}}$.

Pump beams which were oriented in the same manner but had the same type of polarization (both o-waves or both e-waves) did not produce the effects described above.

Additional qualitative and quantitative experimental data will be presented below when the results are compared with the theory.

3. PARAMETRIC SCATTERING GEOMETRY

Suppose that the behavior described above is associated with the $oe \rightarrow oo$ and $oe \rightarrow ee$ parametric processes, satisfying

the phase-matching condition

$$\mathbf{k}_p{}^o+\mathbf{k}_p{}^e=\mathbf{k}_1+\mathbf{k}_2. \quad (1)$$

For the $oe\to oo$ process (which, for brevity, we shall call the o process) the wave vectors $\mathbf{k}_{1,2}$ belong to the ordinary waves, while for the $oe\to ee$ process (the e process) they belong to the extraordinary scattered waves. In accordance with the conditions of the experiment, we assume that the pump wavevectors $\mathbf{k}_p^{o,e}$ lie in the xy plane of the crystal. Unless stipulated otherwise, all waves have the same frequencies.

The equation (1) determines a surface in the space of the wave vectors of the scattered waves for each of the processes, o and e. We employ a spherical coordinate system whose polar axis is oriented in the direction of the vector $\mathbf{k}_p^o+\mathbf{k}_p^e$ and whose azimuthal angle φ is measured from the XY plane. Then, in both o and e processes the scattered wave with wave vector $\mathbf{k}_1$ and the conjugate wave with wave vector $\mathbf{k}_2$ have different polar angles, $\theta_{o,e}^{(1)}=\theta_{o,e}^{(2)}=\theta_{o,e}$ and opposite azimuthal angles $\varphi_1-\varphi_2=\pm\pi$ (Fig. 3). To describe the scattering geometry it is sufficient to prescribe the dependence $\theta_{o,e}(\varphi)$ for $0\leqslant\varphi\leqslant\pi$. From Eq. (1) it is not difficult to obtain for the o and e processes

$$\sin^2\theta_{o,e}=\sin^2\theta_p\pm\xi\cos^2\theta_p, \quad (2)$$

where $\xi=(n_o-n_e)/n_o$ and $n_{o,e}$ are the refractive indices for the o and e waves. The equation (2) was derived under the assumption that birefringence is weak, $|\xi|\ll 1$. This approximation is well justified for $BaTiO_3$ crystals, in which at $\lambda=514$ nm we have $n_o=2.494$ and $n_e=2.431$, i.e., $\xi\approx 0.025$. Thus θ is independent of φ and in both cases we have a circular cone of scattered waves.

Since $\xi>0$ holds, the process $oe\to oo$ is also allowed for arbitrarily small angle θ_p, while the process $oe\to ee$ is possible only for $\theta_p\geqslant\xi^{1/2}$. The scattering angle $\theta_o(\theta_p)$ increases from the value $\theta_o^{\min}=\xi^{1/2}$ in the case of the o process and from zero in the case of the e process. For $BaTiO_3$ we have $\theta_o^{\min}\approx 9$ (the minimum scattering angle in air is equal to 23°). In what follows, unless otherwise stipulated, all values of the polar angles are given inside the crystal.

In the actual case of small-angle scattering, for $\theta^2\ll 1$, Eq. (2) simplifies:

$$\theta_{o,e}^2=\theta_p{}^2\pm\xi. \quad (3)$$

Since we have $\theta_p^2<n_o^{-2}$, refraction at the entrance surface usually ensures that Eq. (3) is applicable for waves inside the crystal.

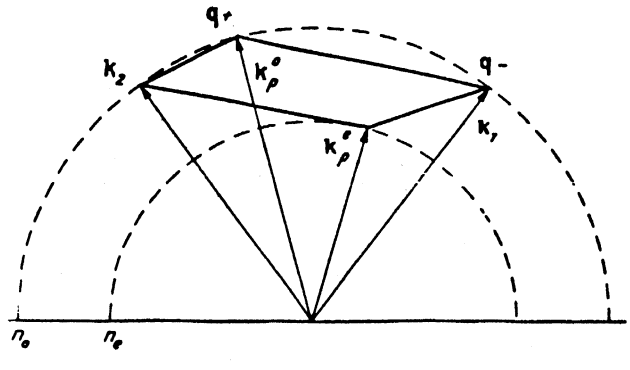

FIG. 3. Diagram of the arrangement of the wave vectors $\mathbf{k}_p^{o,e}$, $\mathbf{k}_{1,2}$, and the lattice vectors $\mathbf{q}_\pm$ for o scattering. The arrangement of the vectors for e scattering is similar.

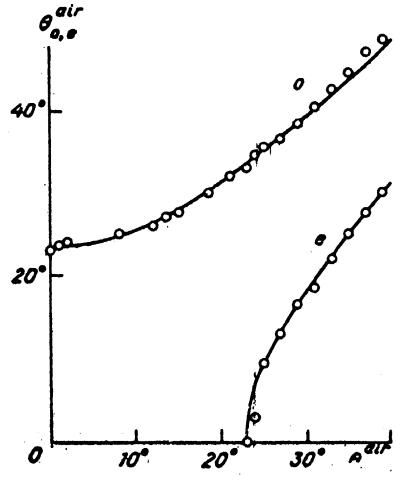

FIG. 4. Angles for the cones of o and e scattering $\theta_{o,e}^{\text{air}}$ as a function of the pump angle θ_p^{air}.

The measurements and the computed dependences $\theta_{o,e}^{\text{air}}(\theta_p^{\text{air}})$ for $BaTiO_3$ are presented in Fig. 4. It is evident that the theory is in quantitative agreement with experiment. Thus the scattering angles, the polarization properties of the scattering, and the threshold angle for the e process have a consistent explanation.

We note that the scattering remains conical outside the crystal only when the vector $\mathbf{k}_p^o+\mathbf{k}_p^e$ is normal to the entrance and exit faces of the crystal, i.e., when the pump waves are incident symmetrically. In the opposite case, refraction distorts the cone.

4. BASIC EQUATIONS

First we give a qualitative interpretation of the parametric scattering. For this, we introduce the vectors $\mathbf{q}_\pm$ of the spatial gratings:

$$\begin{aligned}\mathbf{q}_+&=\mathbf{k}_1-\mathbf{k}_p{}^e=\mathbf{k}_p{}^o-\mathbf{k}_2,\\ \mathbf{q}_-&=\mathbf{k}_1-\mathbf{k}_p{}^o=\mathbf{k}_p{}^e-\mathbf{k}_2,\end{aligned} \quad (4)$$

formed by pairs of waves with $\mathbf{k}_1$, $\mathbf{k}_p^e$ and $\mathbf{k}_p^o$, $\mathbf{k}_2$, on the one hand, and pairs with $\mathbf{k}_1$, $\mathbf{k}_p^o$ and $\mathbf{k}_p^e$, $\mathbf{k}_2$ on the other. To each of the allowed processes (o or e) at a fixed angle φ there is associated a pair of grating vectors $\mathbf{q}_\pm$ (see Fig. 3). Diffraction of the pump waves by the permittivity gratings $\Delta\hat{\varepsilon}(\mathbf{q}_\pm\mathbf{r})$ amplifies the waves 1 and 2 and therefore also the amplitude of the gratings. The initial scattering of the light can thus be amplified. The advantage of waves which satisfy the phase-matching condition lies in the possibility of adding independent gratings and different diffracted beams.

We now describe the parametric scattering. The nonlinear change in the permittivity tensor is associated with the electric field $\mathbf{E}$,

$$\Delta\hat{\varepsilon}_{ij}(\omega)=-n_o{}^3r_{ijl}E_l,$$

where r_{ijl} is the tensor of the linear electrooptic effect.[13] The contribution, corresponding to Eq. (4), to the electric field has the form

$$\mathbf{n}_+E_+\exp(i\mathbf{q}_+\mathbf{r})+\mathbf{n}_-E_-\exp(i\mathbf{q}_-\mathbf{r})+\text{c.c.}, \quad (5)$$

where $\mathbf{n}_\pm = \mathbf{q}_\pm / q_\pm$ are unit vectors and $E_\pm$ are the amplitudes of the gratings. Equations describing the change in the amplitudes $A^{o,e}$ of the waves as a result of diffraction can be derived in the standard manner from Maxwell's equations.[14,15] In writing down the final result we employ the fact that the parameters θ^2 and ξ are small, and we also take into consideration the fact that in $BaTiO_3$ the electrooptic coefficient $r_{51} \equiv r_{131}$, responsible for diffraction with a change in the type of polarization, is more than one and a half orders of magnitude greater than the other independent coefficients $r_{13} \equiv r_{113}$ and $r_{33} \equiv r_{333}$. For the scattered o and e waves 1 and 2 we have

$$\frac{dA_1^o}{dx} = -iS_+^o E_+^o A_p^e, \quad \frac{dA_2^o}{dx} = -iS_-^o \bar{E}_-^o A_p^e, \tag{6a}$$

$$\frac{dA_1^e}{dx} = -iS_-^e E_-^e A_p^o, \quad \frac{dA_2^e}{dx} = -iS_+^e \bar{E}_+^e A_p^o, \tag{6b}$$

where

$$S_\pm = \frac{\pi n_o^3 r_{51}}{\lambda} \frac{\theta \cos\varphi \pm \theta_p}{(\theta^2 + \theta_p^2 \pm 2\theta\theta_p \cos\varphi)^{1/2}}, \tag{7}$$

the angle θ for the o or e process is given by Eq. (3), the angles θ_o or θ_e in $S_\pm$ are determined by the relation (3), the overbar indicates complex conjugation, and the X axis is assumed to be normal to the entrance face of the crystal.

The changes in the amplitudes of the pump waves $A_p^{o,e}$ are given by the following expressions:

$$\begin{aligned} \frac{dA_p^e}{dx} &= -i\int_0^\pi (S_+^o \bar{E}_+^o A_1^o + S_-^o E_-^o A_2^o)\, d\varphi, \\ \frac{dA_p^o}{dx} &= -i\int_0^\pi (S_-^e \bar{E}_-^e A_1^e + S_+^e E_+^e A_2^e)\, d\varphi. \end{aligned} \tag{8}$$

The conservation of the total energy of the waves is expressed by the fact that the quantity I_Σ, defined as

$$I_\Sigma = I_p^o + I_p^e + \int_0^\pi (I_1^o + I_2^o + I_1^e + I_2^e)\, d\varphi \tag{9}$$

is constant. We refer to the squares of the absolute values of the amplitudes ($I_{1,2}^0 = |A_{1,2}|^2$, etc.), appearing in Eq. (9) and below, as the intensities of the separate beams.

In Eqs. (6) and (8) the time derivatives are dropped because of the inertia of the nonlinearity. However the time dependence is contained in the material equations, which express the amplitudes $E_\pm$ of the gratings in terms of the amplitudes of the light waves:

$$\begin{aligned} \left(\frac{d}{dt} + 1\right) E_\pm^o &= I_\Sigma^{-1} (iE_D^\pm - \mathbf{n}_\pm \mathbf{E}_{ex}) \begin{pmatrix} A_p^o & \bar{A}_2^o \\ A_1^o & \bar{A}_p^o \end{pmatrix}, \\ \left(\frac{d}{dt} + 1\right) E_\pm^e &= I_\Sigma^{-1} (iE_D^\pm - \mathbf{n}_\pm \mathbf{E}_{ex}) \begin{pmatrix} A_1^e & \bar{A}_p^e \\ A_p^e & \bar{A}_2^e \end{pmatrix}. \end{aligned} \tag{10}$$

We introduce below the following notation: $\tau = t/t_{di}$ is the dimensionless time, $t_{di}(I_\Sigma)$ is the dielectric relaxation time, $E_D^\pm = q_\pm T/e$ is the diffusion field, e is the electron charge, and $\mathbf{E}_{ex}$ is the external field. It is presumed that the quantities $\mathbf{n}$ and $q_\pm$ appearing in Eq. (10) depend not only on the grating indices but also on the type of process (o or e). It is not difficult to show that

$$q_\pm = \frac{2\pi n_o}{\lambda} (\theta^2 + \theta_p^2 \pm 2\theta\theta_p \cos\varphi)^{1/2}. \tag{11}$$

In deriving Eq. (10) we assumed that absorption is isotropic and we neglected the photogalvanic effect,[6,15] since in undoped $BaTiO_3$ its contribution to the formation of the gratings is small.[16]

We now discuss the characteristic features of parametric scattering which are related to the general properties of Eqs. (6), (8), and (10). In accordance with Eqs. (6) and (8) the electrooptic constant r_{51} gives rise only to diffraction with a change in the type of polarization. For this reason, for the process $oe \to oo$ the increase in the amplitudes of the scattered waves could be related to the depletion of only the e pump wave, while for the process $oe \to ee$ it could be related to the depletion of the o pump beam. In particular, below the threshold of the o process, i.e., for $\theta_p < 9°$, the intensity I_p^o should remain constant. This feature is clearly manifested in the experiment. Thus, for a 2.6-mm-thick sample and $\theta_p^{air} = 14°$ the depletion of the e pump wave reached 75%, while the decrease in the intensity of the o beam, in contrast, was insignificant.

Another consequence of diffraction with a change in polarization is manifested when one of the pump beams is blocked. If after sufficiently prolonged exposure the o pump beam is blocked, then the $E_\pm$ gratings formed cannot disappear instantaneously. For this reason, an appreciable change in the intensity of e scattering (if e scattering is allowed) should not be observed at the exit from the crystal, while the intensity of o scattering should drop instantaneously almost to zero. Conversely, when the e pump beam is blocked o scattering should remain unchanged. These features are fully manifested in the experiment. After one of the pump beams was blocked the $E_\pm$ gratings relaxed over a time comparable to the dielectric relaxation time.

We now consider the material equations (10). It is important that the $E_\pm$ gratings are formed only by pairs of waves of the same type: ordinary waves for the o process and extraordinary waves for the e process. This feature explains why in Eq. (8) we neglected the grating with vector $\mathbf{k}_p^o - \mathbf{k}_p^e$, i.e., the interaction of the pump waves with one another. Now we can also understand why the o and e processes require differently polarized pump waves, while a pump wave of the same type as the scattered waves participates in the formation of the $E_\pm$ gratings and the pump beam with the other type of polarization is diffracted by these gratings. This feature of the material equations (10) in turn follows from the fact that the charge separation due to drift and diffusion of photoelectrons requires modulation of the light intensity.

We note that switching from small scattering angles ($\theta^2 \ll 1$) to finite angles does not qualitatively change the polarization and angular properties of the effect. The need to refine the model for large angles θ (i.e., for large $q_\pm$) is more likely attributable to spatial dispersion effects, which adjust the scattering intensity.[17] Generalizations of this type (as well as some other types) will be given in Sec. 5 in application to the stationary state.

5. STATIONARY SCATTERING IN THE FIXED-PUMP APPROXIMATION

In the stationary state the amplitudes of the scattered waves satisfy the equations

$$\frac{dA_1}{dx} = V_{12}\bar{A}_2 A_p^o A_p^e,$$
$$\frac{d\bar{A}_2}{dx} = \bar{V}_{21} A_1 \bar{A}_p^o \bar{A}_p^e \qquad (12)$$

with the coupling coefficients

$$V_{12}^{o,e} = S_+ (E_D^{\pm} + i\mathbf{n}_\pm \mathbf{E}_{ex})/I_\Sigma,$$
$$V_{21}^{o,e} = -S_\mp (E_D^{\mp} - i\mathbf{n}_\mp \mathbf{E}_{ex})/I_\Sigma. \qquad (13)$$

We have dropped the indices o and e everywhere where doing so would not result in any misunderstandings.

So long as the parametric scattering is relatively weak, we can assume that the amplitudes $A_p^{o,e}$ are constant (fixed pump field approximation). The system (12) then becomes linear and relates A_1 to the complex-conjugate amplitude $\bar{A}_2$. Such a relation is typical for parametric processes.

Assuming $A_1, \bar{A}_2 \propto \exp(\Gamma x)$, we obtain for the growth rate Γ

$$\Gamma = |A_p^o A_p^e| (V_{12}\bar{V}_{21})^{1/2}. \qquad (14)$$

In the general case Γ is a complex quantity; amplification of the scattered waves corresponds to $\mathrm{Re}\Gamma > 0$.

We now investigate the behavior of the growth rates in the most important limiting cases. We consider first the diffusion model, $\mathbf{E}_{ex} = 0$, which corresponds to the conditions of our experiments. Taking into consideration Eqs. (7) and (11), we obtain the following general formula for o and e processes:

$$\Gamma = \beta E_D^m (\theta_p^2 \mp \theta^2 \cos^2\varphi)^{1/2}, \qquad (15)$$

where the coefficient β does not depend on the angles,

$$\beta = \frac{\pi n_0^3 r_{51}}{4\lambda} \frac{2(I_p^o I_p^e)^{1/2}}{I_p^o + I_p^e}, \qquad (16)$$

and $E_D^m = 4\pi n_0 T/\lambda_e$ is the maximum possible diffusion field, induced in the crystal by light with wavelength λ. The difference between the growth rates $\Gamma_{o,e}$ for the o and e processes is connected entirely with the difference between the scattering angles $\theta_{o,e}$, which satisfy the formula (3). The angular dependence of Γ is symmetric relative to reflections in the horizontal plane xy and the vertical plane xz.

As follows from Eq. (15), stationary amplification is possible for the o process only in a limited range of azimuthal angles, $|\cos\varphi| < \theta_p/\theta$, which we shall term the allowed range. Here, evidently, $\Gamma_o > 0$. In the forbidden range of angles ($|\cos\varphi| > \theta_p/\theta$) Γ_o is an imaginary quantity and stationary amplification is impossible. Thus, when the angle between the pump waves is small, $\theta_p \ll \xi^{1/2}$, the scattered o waves are concentrated near $\varphi = \pm\pi/2$; for $\theta_p = \xi^{1/2}$ (i.e., at the threshold of the e process) the region of stationary amplification encompasses the upper and lower fourths of the circle, while for $\theta_p \gg \xi^{1/2}$ the scattered o waves try to fill the entire circle. It is likewise easy to show that this restriction on the angles φ is equivalent to the assertion that only the scattered o waves whose wave vectors lie between the vertical planes passing through $\mathbf{k}_p^o$ and $\mathbf{k}_p^e$ are amplified. The maximum value of the growth rate Γ_o as a function of φ occurs at $\varphi = \pm\pi/2$: $\Gamma_o^m = \beta E_D^m \theta_p$; it increases linearly with θ_p. The behavior of $\Gamma_o(\theta_p, \varphi)$ in the allowed and forbidden intervals of angles is illustrated in Fig. 5a. Note the large absolute values of the growth rate, $\Gamma_o \geqslant 10^2$ cm^{-1}.

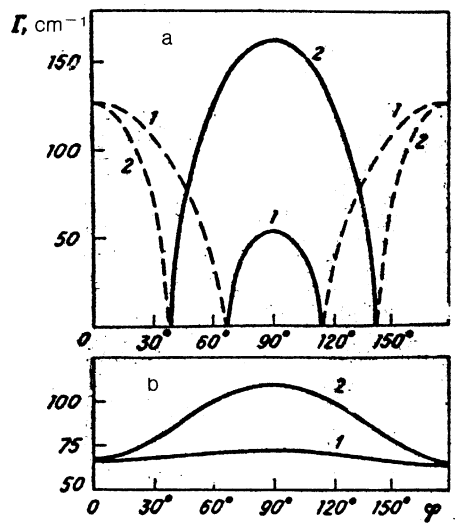

FIG. 5. Computed azimuthal dependences $\Gamma_{o,e}(\varphi)$ for o and e processes with the optimal ratio of the intensities of the pump beams: a) the solid lines depict $\Gamma_o(\varphi)$ in the allowed range of angles and the dashed lines depict $|\Gamma_o(\varphi)|$ in the forbidden range of angles φ for $\theta_p^{\mathrm{air}} = 10°$ (curve *1*) and 30° (curve *2*); b) $\Gamma_e(\varphi)$ for $\theta_e^{\mathrm{air}} = 10°$ (curve *1*) and 30° (curve *2*).

For the e process stationary amplification of the scattered waves occurs for all azimuthal angles φ. Near threshold, when $\theta_e \ll \xi^{1/2}$, the dependence $\Gamma_e(\varphi)$ is weak; for $\theta_e \geqslant \xi^{1/2}$ at the points $\varphi = \pm\pi/2$ there is a pronounced maximum: $\Gamma_e^m = \beta E_D^m \theta_p$ (see Fig. 5b).

Comparing the behavior of $\Gamma_{o,e}(\varphi, \theta_p)$ described above with the results of Sec. 2, we see that all experimental results concerning the azimuthal distribution of o and e scattering and the dependence of the scattering intensity on θ_p can be completely explained on the basis of the diffusion model.

The relations found above for the growth rates $\Gamma_{o,e}$ can be generalized. First we take into account the difference between the absorption coefficients $\alpha_{o,e}$ for o and e waves. For this it is sufficient to replace the factor

$$m = 2(I_p^o I_p^e)^{1/2}/(I_p^o + I_p^e)$$

by

$$m_{o,e} = 2\alpha_{o,e}(I_p^o I_p^e)^{1/2}/(\alpha_o I_p^o + \alpha_e I_p^e).$$

This substitution reflects the fact that the formation of gratings for the o and e processes is associated with the absorption of o and e waves, respectively, while the dielectric relaxation rate is proportional to the total absorption of o and e pump waves. We can see that the coefficient β becomes different for the o and e processes, with $\beta_o/\beta_e = \alpha_o/\alpha_e$. The maximum value of Γ is now reached not for equal pump wave intensities but rather for $\alpha_o I_p^o = \alpha_e I_p^e$. At the maximum $m_{o,e} = \alpha_{o,e}/(\alpha_o \alpha_e)^{1/2}$. In $BaTiO_3$ we have $\alpha_o \approx 1.2$ cm^{-1} and $\alpha_e \approx 0.6$ cm^{-1}, and thus instead of $m = 1$ and $I_p^o = I_p^e$ we have at the maximum $m_o \approx 2^{1/2}$, $m_e \approx 2^{-1/2}$, and $I_p^e \approx 2I_p^o$. The computed curves $\Gamma_{o,e}(\varphi)$ presented in Fig. 5 correspond to this optimal intensity ratio. Figure 6 shows the experimental dependence of the intensity of o scattering on the ratio I_p^o/I_p^e. The position of the maximum is

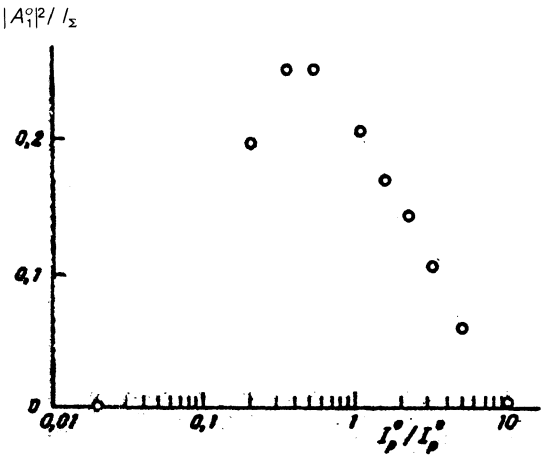

FIG. 6. Integrated intensity of o scattering, normalized to the total intensity of the light incident on the crystal, as a function of the ratio of the intensities of the pump beams.

not symmetric and agrees well with the theoretical prediction.

Another extension of the formulas for the growth rate involves the anisotropy of electron mobility. It can be confirmed that the results obtained on the basis of the diffusion model are valid for an arbitrary ratio of the longitudinal mobility $\mu_\parallel$ and the transverse mobility $\mu_\perp$. The point is that the photoelectron diffusion coefficients $D_{\parallel,\perp}$ are related with the mobilities by the Einstein relations $D_{\parallel,\perp} = T\mu_{\parallel,\perp}/e$ while the diffusion field is determined by their ratio.

The modification of the formulas for the growth rate can be related to spatial dispersion effects. It is known[17] that for sufficiently large photoelectron Debye lengths, $L_D \geqslant 1/q_\pm$, the charge separation decreases, so that $E_D(q) \to E_D(q)/(1+q^2L_D^2)$. For large angles θ_p the spatial dispersion can decrease the intensity of parametric scattering and can be reflected in the azimuthal dependence of the growth rate.

We now consider briefly the other limiting case, $E_{ex} \gg E_D = kT\theta_p/e$. This case can be easily realized experimentally, since the characteristic values of the diffusion field for small-angle scattering are equal to only a few V/cm. Assuming that $\mathbf{E}_{ex}$ is oriented along the z axis, we obtain from Eqs. (7), (13), and (14)

$$\Gamma_{o,e} = \beta E_{ex} f(\theta, \varphi),$$
$$f = 2\theta \sin\varphi [(\theta^2\cos^2\varphi - \theta_p^2)/(\xi^2 + 4\theta^2\theta_p^2\sin^2\varphi)]^{1/2}. \quad (17)$$

The angles $\theta = \theta_o$ and $\theta = \theta_e$ correspond to the o and e processes. Taking into consideration Eq. (3), we find that amplification of the waves is impossible for the e process, while for the o process amplification occurs in the region where it was forbidden in the diffusion model. If $2\theta_p \ll \xi$, then $\Gamma_o(\varphi)$ assumes its maximum values at $\varphi = \pm\pi/4$ and $\varphi = \pm 3\pi/4$, where $f \approx 1/2$. For $2\theta_p \gg \xi^{1/2}$ four symmetric maxima are realized near $\varphi = 0$ and π; here $f \approx 2$. The longitudinal photogalvanic effect should also lead to a similar angular dependence of the growth rate,[6] if the photogalvanic electric field is stronger than the diffusion field.

Although the basic features of the distribution of the scattered waves are determined by the large exponential parameter $\exp(\Gamma x)$, some significant features are associated with the preexponential factor, which is determined by the properties of the initial scattering and the interaction parameters appearing in Eq. (12). On the basis of the fixed-pump approximation it is easy to obtain the general solution for $A_{1,2}$ with arbitrary boundary conditions $A_{1,2}(0) = A_{1,2}(\varphi, x = 0)$. This approach to describing o and e processes corresponds to the situation when the source of the initial scattering is the entrance surface of the crystal. According to Ref. 18, this situation is characteristic for $BaTiO_3$. The initial scattering by volume defects can, in principle, be taken into account by adding small terms on the right-hand side of Eqs. (12). It is obvious from general considerations, however, that even when the initial bulk scattering is predominant waves which were scattered near the front face of the crystal will make the main contribution to the outgoing radiation. We assume that the initial scattering is surface scattering.

In the most important limit, $\exp(\Gamma x) \gg 1$, we have from Eqs. (12) and (14)

$$A_1 = \tfrac{1}{2}\{A_1(0) + \bar{A}_2(0)(V_{12}/V_{21})^{1/2}\exp[i(\Phi_p^o + \Phi_p^e)]\}e^{\Gamma x},$$
$$\bar{A}_1 = \tfrac{1}{2}\{A_1(0)(V_{21}/V_{12})^{1/2}\exp[-i(\Phi_p^o + \Phi_p^e)] + \bar{A}_2(0)\}e^{\Gamma x}, \quad (18)$$

where $\Phi_p^{o,e}$ are the phases of the o and e pump waves. The preexponential factors (in contrast to the growth rate Γ) depend on the ratios of the phases of all four complex quantities $A_p^{o,e}$ and $A_{1,2}(0)$; moreover, they do not exhibit any symmetry properties relative to reflection in the vertical xz plane. The expressions (18) are symmetric only with respect to reflection in the horizontal xz plane. The symmetry of the solution thus corresponds to the symmetry of our problem (see Fig. 1). According to Eq. (18), the ratio of the intensities of mutually conjugate scattered waves is $|A_1/A_2|^2 = |V_{12}/V_{21}|$.

In the diffusion model we have for o and e processes

$$\frac{V_{12}}{V_{21}} = \frac{\theta_p \pm \theta\cos\varphi}{\theta_p \mp \theta\cos\varphi}. \quad (19)$$

For the o process V_{21} and V_{12} in Eq. (18) formally vanish at the boundary of the region of amplification. At the edge of the region of amplification, however, the condition $\exp(\Gamma x) \gg 1$ breaks down and the equations (18) are no longer applicable.

According to Eq. (18), the intensities of the scattered waves $I_{1,2}(\varphi)$ undergo modulation[1)] as a function of the phase $\Phi = \Phi_p^o + \Phi_p^e - \Phi_1(0) - \Phi_2(0)$ of the form $1 + M\cos\Phi$ with modulation factor M:

$$M = 2\left[\frac{|A_1(0)|}{|A_2(0)|}\left(\frac{\theta_p \mp \theta\cos\varphi}{\theta_p \pm \theta\cos\varphi}\right)^{1/2} + \frac{|A_2(0)|}{|A_1(0)|}\left(\frac{\theta_p \pm \theta\cos\varphi}{\theta_p \mp \theta\cos\varphi}\right)^{1/2}\right]^{-1}. \quad (20)$$

At $\varphi = \pm\pi/2$ [which corresponds to the maximum of $\Gamma_o(\varphi)$] we have $I_1 = I_2$ and $M = 1$.

For the o process the main contribution to the initial scattering is most likely associated with the o pump wave, while for the e process it is associated with the e pump wave. We underscore the fact that the dependence of the intensity on the phase Φ presupposes that the phase differences are constant. If temporal or spatial fluctuations are present,

averaging over Φ can occur. Phase dependences have not yet been investigated experimentally.

We now estimate the total intensity of parametric scattering I_s at the exit from the crystal. The main contribution to I_s comes from the neighborhood of the maximum growth rate, and when integrating over the angle φ we can employ the saddle-point method.[20] For the o process we have

$$I_s^o(l) \approx I_s^o(0) \frac{\theta_p}{\theta_0} \frac{\cos^2(\Phi/2)}{(4\pi\Gamma_o^m l)^{1/2}} \exp(2\Gamma_o^m l), \qquad (21)$$

where $I_s^o(0)$ is the initial intensity of the scattered waves and l is the thickness of the crystal. The intensity of e scattering I_s^e differs primarily because Γ_o^m is replaced by Γ_e^m and by the modulation factor $M < 1$.

6. SCATTERING KINETICS

We employ the fixed-pump approximation to describe the transient properties of scattering. This approximation makes it possible to obtain quite simple closed-form expressions for the amplitudes of the scattered waves for arbitrary φ. Here we confine our attention to the o process, which is distinguished by a large variety of transient states, and to the diffusion model for the coupling coefficients V_{12} and V_{21}.

After Laplace-transforming[20] with respect to the variables x and τ, the system of equations (6a) and (10) becomes an algebraic system. Solving this linear algebraic system and using tables of the inverse Laplace transform,[21] we obtain

$$A_1(x,\tau) = A_1(0) + \left(\frac{\Gamma x}{4}\right)^{1/2} \int_0^\tau e^{-t} \left\{ A_1(0) I^+ + \bar{A}_2(0) \left(\frac{V_{12}}{V_{21}}\right)^{1/2} \exp[i(\Phi_p^o + \Phi_p^e)] I^- \right\} \frac{dt}{t^{1/2}},$$
$$I^\pm = I_1(2[\Gamma x t]^{1/2}) \pm J_1(2[\Gamma x t]^{1/2}), \qquad (22)$$

where $J_1(x)$ and $I_1(x)$ are first-order ordinary and modified Bessel functions. An expression for $\bar{A}_2$ can be easily found from Eq. (22) with the help of symmetry considerations. The formula (22) can be employed both in the allowed interval of azimuthal angles, where $\Gamma_o > 0$, and in the forbidden region, where $\Gamma_o(\varphi)$ is imaginary. From Eq. (22) it can be shown that for $\exp(\Gamma x) \gg 1$ and $\tau \to \infty$ the amplitude A_1 approaches the stationary value (19).

The scattering kinetics described by Eq. (22) changes radically when we pass from the allowed into the forbidden range of angles. In the allowed region, where $\exp(\Gamma x) \gg 1$, the modified Bessel functions make the main contribution to the integral. Assuming that the scattering is strong enough so that $|A_1| \gg |A_1(0)|$, it is easy to obtain from Eq. (22)

$$|A_1| = \left| |A_1(0)| + |A_2(0)| \left(\frac{\theta_p + \theta\cos\varphi}{\theta_p - \theta\cos\varphi}\right)^{1/2} e^{i\Phi} \right| F_0(\Gamma x;\tau)/2, \qquad (23)$$

where

$$F_0 = \int_0^{2(\Gamma x\tau)^{1/2}} \exp\left(-\frac{\xi^2}{4\Gamma x}\right) \frac{d}{d\xi} I_0(\xi)\, d\xi,$$

and $I_0(\xi)$ is the zeroth-order modified Bessel function. One can see that the right-hand side of Eq. (23) is a product of two factors. The first factor gives the same dependence of A_1 on the phase difference $\Phi = \Phi_p^o + \Phi_p^e - \Phi_1(0) - \Phi_2(0)$, the azimuthal angle φ, and $|A_{1,2}(0)|$ as the stationary relation (19). The entire dependence on x and τ is contained in the factor F_0; as $\tau \to \infty$ we have $F_o \to F_o(\infty) = \exp(\Gamma x)$. Figure 7 shows plots of the quantity $|F_o(\tau)/F_o(\infty)|^2$ for different values of Γx. They show that stationary scattering is established in the allowed interval monotonically with a characteristic time which is significantly longer than the dielectric relaxation time t_{di} and increases almost linearly with Γx.

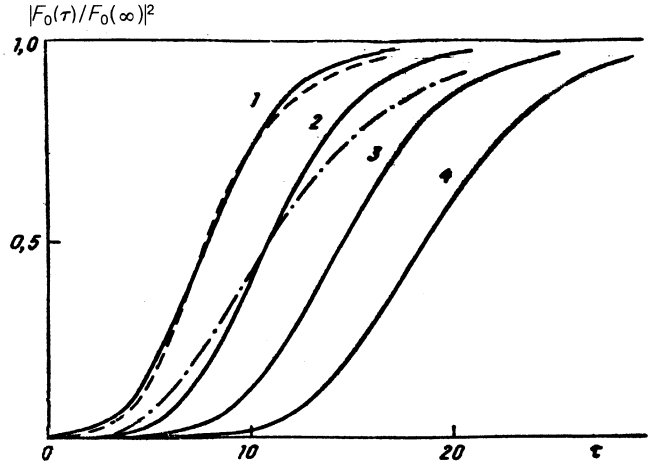

FIG. 7. Computed time dependence of the reduced intensity of o scattering in the allowed interval of angles for $\Gamma l = 6.25$, 9, 12, 25, and 16 (solid lines from *1* to *4*, respectively). The value $\Gamma l = 6.25$ corresponds to the conditions of the experiment with $\theta_p^{\text{air}} = 5°$. The dashed and dot-dashed lines were obtained by fitting the experimental data for $\theta_p^{\text{air}} = 5°$ to the theory (see text).

In the allowed interval, where $\exp|\Gamma x| \gg 1$ and $|A_1| \gg |A_1(0)|$, the formula (22) gives

$$|A_1| = \left| |A_1(0)| F_r + |A_2(0)| \left(\frac{\theta\cos\varphi + \theta_p}{\theta\cos\varphi - \theta_p}\right)^{1/2} F_i e^{i\Phi} \right|, \qquad (24)$$

where

$$F_{i,r} = \int_0^{2(|\Gamma|x\tau)^{1/2}} \exp\left(-\frac{\xi^2}{4|\Gamma|x}\right) \frac{d}{d\xi} \begin{pmatrix} \text{bei} \\ \text{ber} \end{pmatrix} d\xi,$$

bei(ξ) and ber(ξ) are zeroth-order Kelvin functions.[16] It is significant that both the ordinary and modified Bessel functions are equally important in the formula (22). In the limit $\tau \to \infty$ the functions $F_{i,r}$ become the trigonometric functions $\sin|\Gamma x|$ and $\cos|\Gamma x|$. For this reason, in accordance with the results of Sec. 5, there is no stationary scattering in the forbidden range of angles.

In contrast to Eq. (23), the formula (24) cannot be represented in the form of factors which depend on x, τ and on φ, Φ, and $|A_{1,2}(0)|$. For this reason, the character of the transient processes can depend here not only on $|\Gamma|x$, but also on the difference Φ of the phases of the waves, the azimuthal angle φ, and the initial amplitudes $|A_{1,2}(0)|$. The dependences on $|\Gamma|x$ and Φ are most interesting. For this reason, we set

$$|A_1(0)| = |A_2(0)| = |A(0)|, \cos\varphi = \pm 1,$$

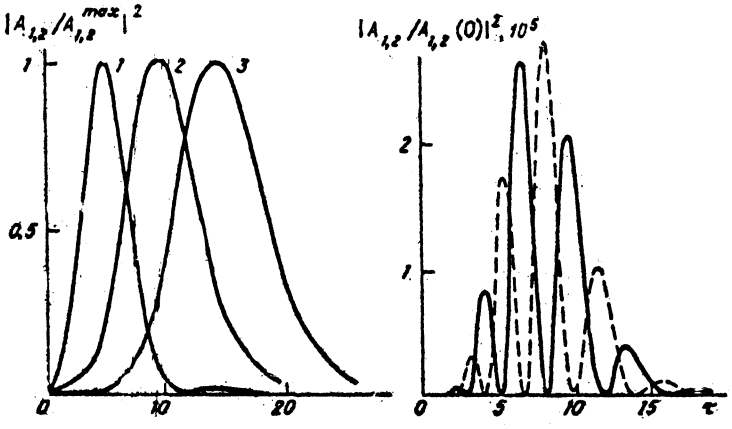

FIG. 8. Computed kinetic curves for the forbidden interval of azimuthal angles, corresponding to the formula (25): a) time dependence of the scattering intensity, normalized to the maximum value with $\Phi = \pm \pi/2$ and $|\Gamma|l = 10$, 20, and 30 (*1*, *2*, and *3*, respectively); b) time dependence of $|A_{1,2}/A_{1,2}(0)|^2$ for $\Phi = 0$ (solid line) and $\Phi = \pi$ (dashed line) for $|\Gamma|l = 16$.

which corresponds to the maximum of $|\Gamma(\varphi)|$, and we confine our attention to the case $\theta^2 \ll \xi$. Under these assumptions, we have for the scattering intensity from Eq. (24)

$$|A_1/A_1(0)|^2 \approx |F_r + F_i e^{i\Phi}|^2. \tag{25}$$

The results of numerical calculations based on the formula (25) for $\Phi = 0$ and π are presented in Fig. 8. For $\Phi = \pm \pi/2$ (see Fig. 8a) the scattering is characterized by one bell-shaped maximum, while at $\Phi = 0$ and π (Fig. 8b) the intensity oscillates many times, the number of oscillations increasing with $|\Gamma|x$. These oscillations correspond to energy transfer from the scattering wave 1 into the conjugate wave 2 and vice versa. Thus the curves *1* and *2* in Fig. 8b describe not only $|A_1/A_1(0)|^2$ for $\Phi = 0$ and π, but also $I_2/I_2(0)$ for $\Phi = \pi$ and 0. The total intensity of the waves 1 and 2 is the same as in the case $\Phi = \pm \pi/2$, when there are no oscillations. The averaging over the phase Φ in Eq. (25) is likewise equivalent to the case $\Phi = \pm \pi/2$. For arbitrary Φ, φ, $|A_1(0)/A_2(0)|$, and θ_p the formula (24) leads to situations which are intermediate with respect to those depicted in Figs. 8a and b. Figure 8a also demonstrates the dependence of the transient scattering on $|\Gamma|x$. One can see that as $|\Gamma|x$ increases the maximum becomes broader and shifts almost linearly in the direction of higher values of τ; the intensity of the transient scattering increases with $|\Gamma|x$ according to a power law. We recall that in the forbidden interval of angles $|\Gamma(\varphi)|^m$ does not depend on θ_p, while in the allowed interval $\Gamma^m \approx \theta_p$. For this reason, for sufficiently small angles θ_p the transient scattering should be stronger than the stationary scattering. The situation reverses as θ_p increases.

The character of the transient processes in the forbidden region of angles contrasts sharply with existing ideas about the amplification of waves as a result of the diffusion nonlinearity.[2,5] It was customarily believed, on the basis of investigations of other optical schemes (both two- and four-beam), that the diffusive nonlinearity leads only to a monotonic increase in the intensity up to stationary scattering. Oscillating dependences of the intensity of the scattered light on the exposure time were observed in parametric scattering in copper-doped $LiNbO_3$ (Ref. 22), but these dependences stem primarily from the local character of the response in this crystal. The difference of our results from previous results is connected with the nontrivial interference effects which occur in our optical scheme.

We now compare the results of the kinetic calculations with experiment. First of all, the diffusion model explains the intense transient scattering in the forbidden region of angles with maxima at the points $\varphi = 0$ and π. The facts that a stationary value is reached monotonically in the allowed region and that there is no scattering for $|\cos\varphi| \approx \theta_p/\theta_0$ agree qualitatively with the theory. The characteristic times of the transient processes, as expected, are approximately an order of magnitude longer than the Maxwell relaxation time of the charge.

No significant oscillations in the intensity of the scattered waves were observed in the forbidden interval. Transient scattering was characterized by a single pronounced maximum. The fact that the theoretically allowed oscillations do not occur is most likely connected with the effective phase averaging as a result of the angular divergence of the beams and the speckle structure of the laser radiation.

Appealing to the case $\Phi = \pm \pi/2$ and Fig. 8a in the forbidden region, we can arrive at very detailed agreement between theory and experiment. Thus for $\varphi = 0$ and π the transient processes do not depend on θ_p. Stationary scattering is established first at the periphery of the allowed interval and only then at the center of the interval, where $\Gamma(\varphi)$ is maximum. The ratio of the time of the transient maximum for $\varphi = 0(\pi)$ and the time over which a stationary value is established for $\varphi = \pi/2$ as well as the ratio of the transient and stationary scattering intensities are in reasonable agreement with the diffusion model for $BaTiO_3$.

An example of the fit between the experimental data and the theory is given in Fig. 7. The fit was made by changing only the horizontal scale (t_{di} was not determined accurately enough). The value of the parameter $\Gamma l = 6.25$ for the theoretical curve (dashed curve) was obtained as a result of direct calculations for the parameters for $BaTiO_3$ and the conditions of the experiment. The experimental curves are obviously in good agreement with the computed curves. An attempt to fit the experiment to the theoretical curve with a "foreign" value of Γl resulted in significantly worse results (see Fig. 7, dot-dashed line).

7. CONCLUSIONS

First we summarize the results obtained. Two new types of photoinduced scattering of light were discovered in photorefractive $BaTiO_3$ crystals. The most striking and significant features of the effects—their high intensity and specific angular, polarization, and kinetic properties—were ex-

plained consistently on the basis of a parametric interaction model. A number of additional scattering features were predicted.

The mechanism which we considered for the spatial amplification of conjugate parametric *o* waves was found to be very effective in optical schemes with phase conjugation.[23] On the basis of the results obtained, it can be expected that further progress will be made in the investigation of nonlinear optical phenomena in $BaTiO_3$ and in understanding the nature of the initial scattering of light and mechanisms of electron-hole transport.

The outlook for constructing a complete picture of parametric scattering in photorefractive crystals and reinterpretation of the role of such effects in the general conception of photoinduced scattering appears to be realistic. This is based on the fact that self-induced scattering in the form of bright lines and dots occurs widely as well as on the fact that these processes have a significant efficiency.

We thank E. Kraetzig and T. Tschudi as well as L. Holtmann, R. Jungen, and W. van Olfen for helpful discussions of the questions touched upon in this paper.

[1)] The dependence of the dissipation of the pump energy on the phase relations is typical for parametric processes.[19]

[1] P. Guenter, Phys. Rep. **93**, 199 (1982).
[2] *Photorefractive Materials and Their Applications. Topics in Applied Physics*, Springer Verlag, Heidelberg (1988, 1989), Vols. 61 and 62.
[3] B. Ya. Zel'dovich, N. F. Pilipetskii, and V. V. Shkunov, *Phase Conjugation* [in Russian], Nauka, Moscow, 1985.
[4] S. G. Odulov, M. S. Soskin, and A. I. Khizhnyak, *Lasers Based on Dynamical Gratings* [in Russian], Nauka, Moscow, 1990.
[5] S. K. Kwong, M. Cronin-Golomb, and A. Yariv, IEEE J. **QE-22**, 1508 (1986).
[6] B. I. Sturman and V. M. Fridkin, *Photogalvanic Effect and Related Phenomena* [in Russian], Nauka, Moscow, 1992.
[7] R. Magnussen and T. K. Gaylord, Appl. Opt. **13**, 1646 (1974).
[8] R. Grousson, S. Mallick, and S. Odoulov, Opt. Commun. **51**, 342 (1984).
[9] I. N. Kiseleva, V. V. Obukhovskii, and S. G. Odulov, Fiz. Tverd. Tela **28**, 2975 (1986) [Sov. Phys. Solid State **28**, 1673 (1986)].
[10] S. Odoulov, J. Opt. Soc. Am. B **4**, 1335 (1987).
[11] S. Odoulov, B. Sturman, L. Hiltmann, and E. Kraetzig, Appl. Phys. B **52**, 317 (1991).
[12] A. Novikov, S. Odoulov, R. Jungen, and T. Tschudi, Opt. Lett. **16**, No. 24 (1991).
[13] Yu. I. Sirotin and M. P. Shaskol'skaya, *Fundamentals of Crystal Physics* [in Russian], Nauka, Moscow, 1979.
[14] B. I. Sturman, Kvantovaya Elektron. **7**, 483 (1980) [Sov. J. Quantum Electron. **10**, 286 (1980)].
[15] S. G. Odulov and B. I. Sturman, Zh. Eksp. Teor. Fiz. **92**, 2016 (1987) [Sov. Phys. JETP **65**(6), 1134 (1987)].
[16] L. Holtmann, E. Kraetzig, and S. Odoulov, Appl. Phys. B **53**, 1 (1991).
[17] N. Kukhtarev, V. Markov, S. Odoulov *et al.*, Ferroelectrics **22**, 949 (1979).
[18] T. Tschudi, A. Herden, J. Goltz *et al.*, IEEE J. **QE-22**, 1493 (1986).
[19] D. N. Klyshko, *Photons and Nonlinear Media* [in Russian], Nauka, Moscow, 1986.
[20] M. A. Lavrent'ev and B. V. Shabat, *Methods in the Theory of Functions of a Complex Variable* [in Russian], Nauka, Moscow, 1965.
[21] A. Erdelyi (ed.), *Tables of Integral Transforms* Vol. 1., McGraw-Hill, New York, 1954.
[22] K. N. Zabrotsin and A. N. Penin, Kvantovaya Elektron. **18**, 622 (1991) [Sov. J. Quantum Electron. **21**, 565 (1991)].
[23] S. Odoulov, B. Sturman, L. Holtmann, and U. van Olfen, Appl. Phys. B **54**, No. 4 (1992).

Translated by M. E. Alferieff